Special Feature: Advanced Alloy Design and Processing of Metallic Materials for Weight- and Energy-saving of Automobiles

Research Report

Formation Behavior of Heterogeneous Cold Deformation Structures That Give Fe-24 wt%Ni-base Alloys Ultra-high Strength and High Ductility

Tadahiko Furuta, Izuru Miyazaki, Keiichiro Oh-ishi and Shigeru Kuramoto

Report received on May 25, 2018

ABSTRACT The formation behavior of heterogeneous cold deformation structures in Fe-24 wt% Ni-base alloys is studied. Ultra-high yield and tensile strengths of approximately 1400 MPa and a high ductility of about 40% are obtained. The alloys were designed to exhibit lattice softening, with $(C_{11}\text{-}C_{12})/2$ and C_{44} at approximately 0 (where C_{11}, C_{12}, and C_{44} are the shear moduli) and low stacking fault energies. The starting temperature of martensitic transformation was around ambient temperature. The critical shear stresses caused by the multimodal deformation processes below the fracture stress, namely dislocation gliding, deformation twins, and stress-induced martensitic transformation, appear to be responsible for the high ductility at an ultra-high stress level. These deformation processes operated simultaneously and successively, not only in the cold working process, but also in the tensile tests. The heterogeneous microstructures formed during cold working are believed to also have played an important role in promoting multimodal deformation in the tensile tests. Detailed microstructural observations were performed to understand the formation mechanism of the heterogeneous microstructure during cold working and plastic deformation behavior at an ultra-high strength level during tensile tests, which was accompanied by a characteristic large Lüders-like deformation.

KEYWORDS Lattice Softening, Ultra-high Strength, Heterogeneous Microstructure, Multimodal Deformation, Stress-induced Martensitic Transformation, Deformation Twinning

1. Introduction

The development of high-strength materials allows weight to be reduced by down-sizing components. Since strengthening usually deteriorates the toughness and ductility of materials, a lot of effort has been devoted to obtaining a good combination of strength (e.g., 1500 MPa) and ductility (e.g., 20%) at ambient temperature. For example, transformation-induced plasticity (TRIP)[1] and twinning-induced plasticity (TWIP)[2,3] have been utilized to obtain a good combination of strength and toughness or ductility owing to their ability to enhance work-hardening capacity. However, it is extremely difficult to combine ultra-high yield strength and high ductility because work-hardening capacity is limited in TRIP and TWIP materials.

Our group has developed some alloys with ultra-high yield strength and high ductility obtained by the alloy-design with elastic lattice softening, which refers to the elastics state where $C' = (C_{11}\text{-}C_{12})/2$ approaches zero; C_{11} and C_{12} denote the elastic constants of the cubic crystals, including β-Ti alloy (GUM METAL),[4-9] nano-structured Fe-Ni-Co-Ti alloys,[10,11] and cold-worked Fe-Ni-Al-C-based alloys.[12] In these alloys, deformation proceeds continuously without macroscopic plastic instability even under ultra-high stress levels. For example, the cold-rolled Fe-24.6%Ni-5.8%Al-0.44%C alloy (compositions are given in wt% unless otherwise stated) has an ultra-high yield strength of approximately 2000 MPa and a tensile elongation of as large as 30% at ambient temperature.[12] To explain the outstanding strength-ductility combination of cold-worked Fe-Ni-Al-C-based alloys, we have recently proposed a multimodal deformation mechanism,[13] which is activated by simultaneous or successive operation of

multiple deformation mechanisms, namely dislocation gliding, deformation twinning, and stress-induced martensitic transformation.[13]

In the present study, the formation behavior of the complex heterogeneous deformation structure that forms during cold-working in Fe-24% Ni-base alloys, which resulted in an ultra-high yield strength of about 1400 MPa and a high ductility of about 40%, was studied. Detailed microstructural observations were conducted using optical microscopy (OM), scanning electron microscopy (SEM), transmission electron microscopy (TEM) and scanning transmission electron microscopy (STEM) from micro to nano regions to understand the microstructural changes during cold working and the plastic deformation during tensile tests.

2. Experimental Procedure

2. 1 Materials

The chemical compositions of the studied alloys are given in **Table 1**. All the samples are Fe-24%Ni-0.45%C-base alloys. A detailed description of alloy design and lattice softening can be found elsewhere.[12] The sample coded 4Al-CR contains 4% Al and samples coded 6Al-CR and 6Al-SW contain 6% Al. CR and SW denote cold rolling and swaging, respectively. The alloys were induction-melted under an argon atmosphere and cast into an iron mold. The ingot was hot-forged at 1423 K into a round bar, 15 mm in diameter, and then solution-treated at 1373 K for 86.4 ks. For the samples 4Al-CR and 6Al-CR, 6-mm-thick plates were taken from the bars, and subjected to cold rolling to 1 mm in thickness. For the sample 6Al-SW, a round bar 12 mm in diameter was taken from the forged bar and cold-swaged to 4 mm in diameter. The equivalent strains, ε_{CR} for cold rolling (CR) and ε_{SW} for cold swaging (SW), are given by the following equations:

Table 1 Test samples.

Sample	Chemical composition (wt%)				The equivalent strain by cold working
	Ni	Al	C	Fe	
4Al-CR	24.1	4.06	0.43	bal.	0-2.07
6Al-CR	23.8	5.98	0.50	bal.	2.07
6Al-SW	24.0	5.01	0.47	bal.	2.20

$$\varepsilon_{CR} = -1.15 \ln (t/t_0) , \quad (1)$$

$$\varepsilon_{SW} = -\ln (S/S_0) , \quad (2)$$

where t_0 and t are the thicknesses before and after cold rolling, respectively, and S_0 and S are the cross-sectional area before and after cold swaging, respectively. For example, an area reduction of 83.3% corresponds to an ε_{CR} of 2.07. The equivalent strains for cold working are also given in Table 1.

2. 2 Tensile Tests

Flat tensile specimens, 6.5 mm in width and 0.8 mm in thickness, and smooth cylindrical specimens, 2.4 mm in diameter and 14 mm in gauge length, were machined from the CR and SW samples, respectively. Tensile tests were performed with an initial strain rate of 5×10^{-4} s^{-1} at room temperature. Two strain gauges were attached to the parallel portion of the specimen surface. For the CR samples, the tensile axis was parallel to the rolling direction (RD).

2. 3 Microstructural Observations and Analysis

Microstructural changes during cold rolling and tensile tests in the sample coded 4Al-CR were observed using OM, SEM with an acceleration voltage of 15 kV, TEM, and STEM with an acceleration voltage of 200 kV. Thin foil samples for TEM and STEM were prepared using a focused ion beam (FIB) machine. The crystallographic orientations were determined using electron backscattered diffraction (EBSD) in SEM and transmission EBSD (t-EBSD). The orientation data were acquired at step sizes of 0.2 and 2 μm; data with a confidence index of less than 0.1 were ignored. Inverse pole figures (IPFs), image quality (IQ), and phase maps were utilized to analyze the deformation behavior during cold rolling.

3. Results

3. 1 Tensile Properties

Figure 1 shows the engineering stress-strain curves for the samples. The sample coded 6Al-SW showed the highest yield strength (about 2100 MPa). All the curves showed similar characteristics, i.e., ultra-high yield strength and a yield drop, followed by

a plateau with primary Lüders-like deformation, work hardening, and secondary Lüders-like deformation, and finally failure. The plastic deformation proceeded continuously without plastic instability under such high stress levels.

3. 2 Microstructural Change with Cold Reduction

Figures 2(a) and (b) show optical micrographs for the solution-treated 6% and 4% Al alloys, respectively. The 6% Al alloy consisted of the face-centered cubic (fcc) (γ) matrix and fine particles of the B2 phase (FeNiAl), whereas the 4% Al alloy consisted of only the γ phase. The grains of γ in the 6% Al alloy were much finer than those in the 4% Al alloy due to the pinning effect of the B2 particles. The 4% Al alloy was selected for investigating the deformation mechanism of the fcc (γ) matrix during cold rolling and tensile tests.

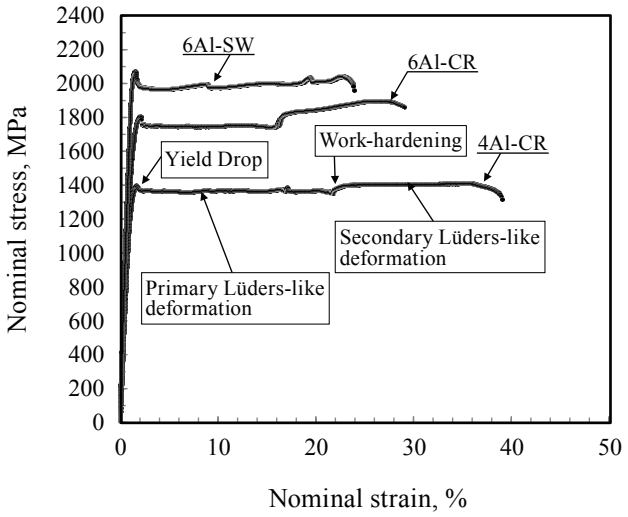

Fig. 1 Engineering stress-strain curves.

Figure 3 compares the optical microstructures of the solution-treated and cold-rolled 4% Al alloy samples. The equivalent strain, ε_{CR}, caused by cold rolling was 2.07. Very coarse grains (over 100 μm) were observed in the solution-treated sample (Fig. 3(a)). The cold-rolled sample showed a quite heterogeneous microstructure. The morphology of the microstructure was classified into one of three types, namely A, B, or C, as shown in Fig. 3(b). Type-A refers to plain microstructures without any characteristic features, elongated along RD. Type-B refers to band-like defects that are approximately 45° to the normal direction (ND). Type-C refers to structures with featureless severe plastic deformation.

The change in microstructural features with ε_{CR} captured by EBSD IPFs for the 4% Al alloy is shown in **Fig. 4**. Crystallographic rotation of several degrees inside grains via dislocation gliding can be observed in the deformed structure with a small cold strain of $\varepsilon_{CR} = 0.12$ (Fig. 4(b)). Deformation twins can be clearly observed for strain (ε_{CR}) values of more than 0.59 (Figs. 4(c) and (d)). Figure 4(e) shows a magnified view of the Type-B microstructure, obtained at an ε_{CR} of 1.06. The misorientation profiles along the red line in Fig. 4(e) indicate that the deformation mechanism of the Type-B structure is twinning, with a misorientation to the neighboring region of about 60° (Fig. 4(f)). In addition, a more deformed region, denoted as Type-C in Fig. 4(d), increased for strain (ε_{CR}) values of more than 1.06; the characteristics of this region could not be analyzed using SEM/EBSD. t-EBSD was thus used for a detailed microstructural analysis of the more deformed structure obtained at a strain (ε_{CR}) of 2.07.

Figure 5(a) shows a bright-field (BF) image obtained using STEM. The microstructure consists

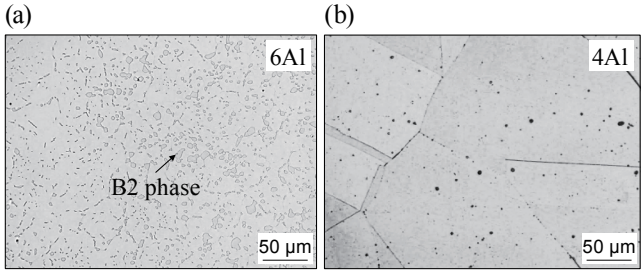

Fig. 2 Optical microstructures of as-solution treated samples. (a) Fe-23.8%Ni-6.01%Al-0.47%C, (b) Fe-24.1%Ni-4.06%Al-0.43%C.

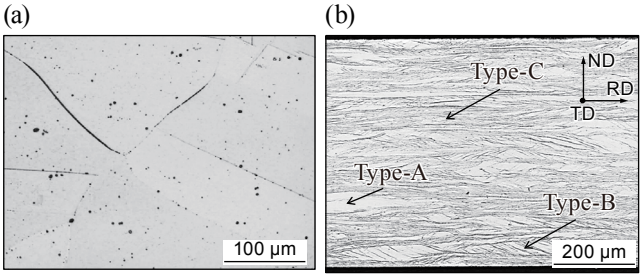

Fig. 3 Optical microstructures of Fe-24.1%Ni-4.06%Al-0.43%C alloy. (a) As-solution treated, (b) cold rolled to ε_{CR} of 2.07.

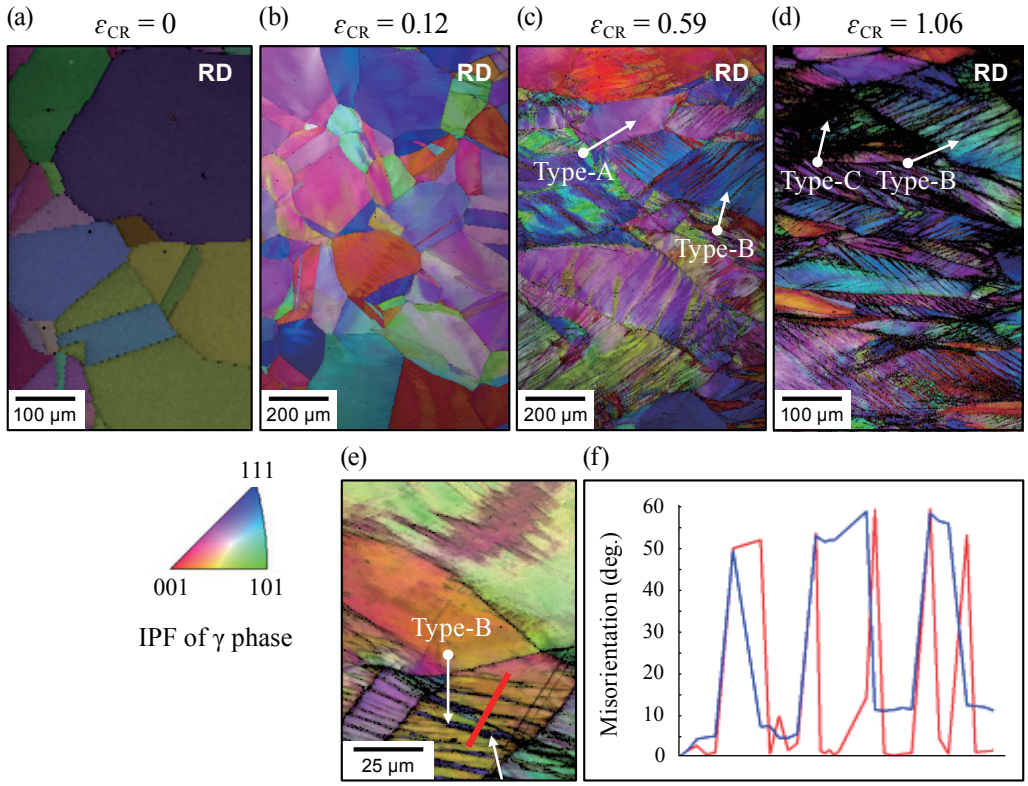

Fig. 4 IPF maps showing change in microstructures of the 4Al-CR samples with an increase in the equivalent strain, ε_{CR}. (a) ε_{CR} = 0, (b) ε_{CR} = 0.12, (c) ε_{CR} = 0.59, (d) ε_{CR} = 1.06, (e) magnified view for ε_{CR} = 0.59, (f) misorientation plots along the red line in Fig. 4(e).

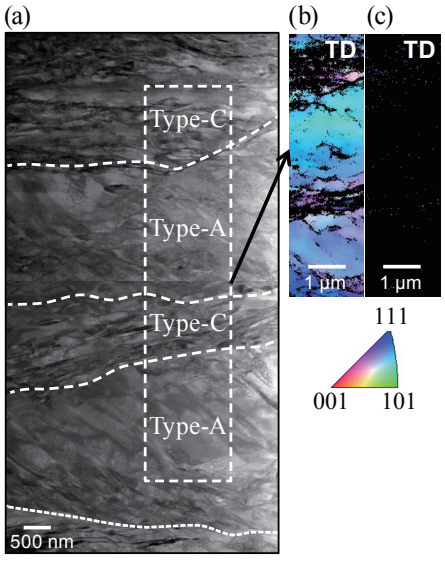

Fig. 5 Microstructure of the 4Al-CR sample cold rolled to ε_{CR} = 2.07. (a) BF-STEM image, (b) IPF map for the γ phase, (c) IPF map for the α' phase.

of Type-A and Type-C regions. Figure 5(b) shows the IPF map corresponding to rectangle region indicated the broken-line in Fig. 5(a). This map shows almost a monolithic crystallographic structure with {110} <001>$_{\gamma}$,[12] without any high-angle boundaries and twin boundaries in the Type-A structure. The phase map reveals that no α'-martensite phase formed in this sample (Fig. 5(c)).

Figure 6(a) shows another BF STEM image. The IPF map reveals that the Type-C structure also consisted of a monolithic crystallographic structure (Fig. 6(b)) with {110}<112>$_{\gamma}$[12] suggesting deformation via dislocation gliding. A small amount of α'-martensite was detected in the Type-C structure, as shown in the phase map of Fig. 6(c). The α'-martensite is formed during severe plastic deformation, i.e., it was stress-induced martensite. Although the volume fraction of α'-martensite obtained at a strain (ε_{CR}) of 2.07 has been reported to be as much as 32.3%,[13] the amount of α'-martensite detected by t-EBSD in this study was much smaller than this value. The very fine α' phase is formed in the heavily deformed region

in Type-C by dislocation glide in this case as shown in **Fig. 7**(a), and the existence of that was confirmed in SAED pattern in Fig. 7(c). This observation results suggest that the γ-to-α' transformation need the high ε_{CR} such as 2.07 during cold rolling.

Deformation twins were also identified in the Type-C structure. **Figures 8**(a) and (b) show dark-field images and Fig. 8(c) shows a SAED pattern. High-lighted thin lamellar structures as shown in Figs. 8(a) and (b) correspond to the diffraction spots T1 and T2 in Fig. 8(c), respectively, which indicate ultra-fine deformation twins.

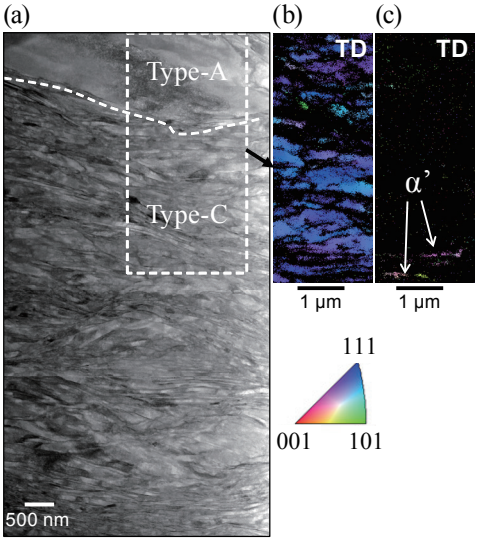

Fig. 6 Microstructure of the 4Al-CR sample cold rolled to ε_{CR} = 2.07. (a) BF-STEM image, (b) IPF map for the γ phase, (c) IPF map for the α' phase.

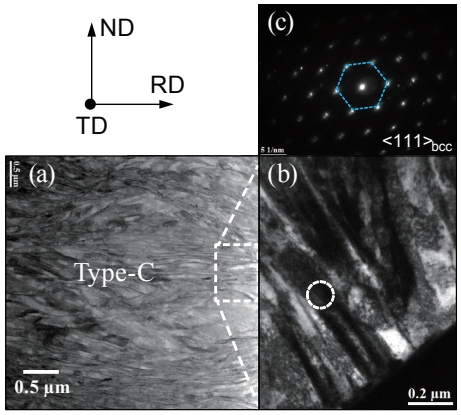

Fig. 7 Type-C microstructure in the 4Al-CR sample cold rolled to ε_{CR} = 2.07. (a) BF-STEM image, (b) TEM image for the square in Fig. 6(a), (c) SAED pattern for the circle in Fig. 7(b).

Based on the detailed microstructural observations, a multimodal deformation mechanism, in the forms of dislocation gliding, deformation twins, and stress-induced martensite, is considered to be activated in the Type-C structure during cold rolling.

3. 3 Microstructural Change during Tensile Tests

The 4% Al alloy severely deformed by cold rolling showed an ultra-high yield strength (about 1400 MPa) and high ductility (total elongation of about 40%), as shown in Fig. 1. The stress-strain curve shows characteristic features, such as primary Lüders-like deformation (as much as 20%), work hardening, and secondary Lüders-like deformation at a very high stress level of about 1400 MPa. The changes in microstructure in the tensile tests were observed using SEM and t-EBSD.

Figure 9(a) shows a SEM image of a cold-rolled sample before the tensile test. Type-A and Type-B

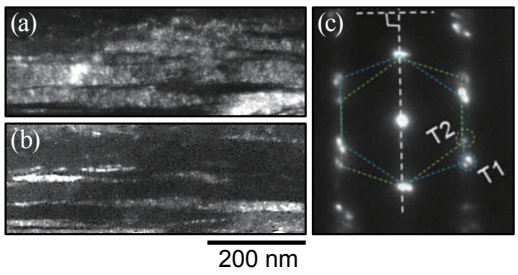

Fig. 8 Dark field (DF) TEM image for the Type-C microstructure in the 4Al-CR sample cold rolled to ε_{CR} = 2.07: (a) DF image corresponding to the T1 spot in Fig. 8(c). (b) DF image corresponding to the T2 spot in Fig. 8(c). (c) SAED pattern.

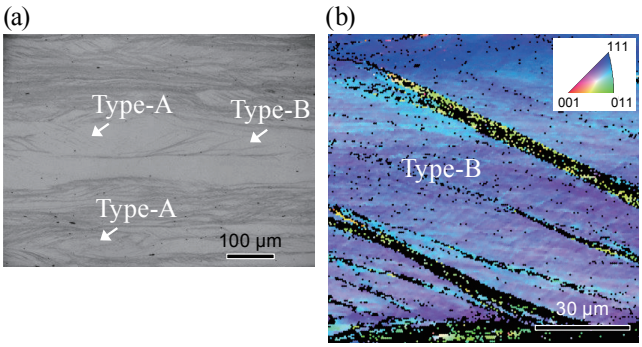

Fig. 9 Microstructure of the 4Al-CR sample before the tensile test. (a) SEM image, (b) IPF map for Type-B structure.

structures appear in this sample. The strain (ε_{CR}) accumulated during cold rolling before the tensile test was 2.07. Figure 9(b) shows the Type-B structure in the sample before the tensile test observed using EBSD.

The microstructural observation results for the fractured tensile specimen are shown in **Fig. 10**. Figure 10(a) shows a low-magnification SEM image of the cross-section near the fractured portion. Careful observations reveal that the region near the fractured portion exhibits secondary Lüders-like deformation bands, and that the remaining regions exhibit primary Lüders-like deformation bands. Figure 10(b) shows a magnified SEM image corresponding to the rectangle in Fig. 10(a) in the primary Lüders-like deformation bands. Fine and dense deformation twins were identified. Figure 10(c) shows a highly magnified IPF map corresponding to the square in Fig. 10(b). Besides the fine and dense deformation twins, activation of stress-induced martensite can be observed in this figure. It should be noted that the fine and dense deformation twins preferentially formed in the Type-A structure, and that the stress-induced martensitic transformation seemed to occur near the boundaries between Type-A and Type-C structures, and inside the Type-C structure.

Figure 10(d) shows a magnified SEM image corresponding to the rectangle in Fig. 10(a) in the secondary Lüders-like deformation bands. The severely deformed structure was too fine to analyze at this magnification. Figure 10(e) shows a highly magnified SEM image corresponding to the rectangle in Fig. 10(d). Ultra-fine dense deformation twins can just barely be seen at the elongated deformation structure near the fractured portion. These ultra-fine twins appear to have formed even in the Type-C structure. A comparison of the ultra-fine uniform deformation structure shown in Fig. 10(d) with those in Figs. 9(a) and 10(b) suggests that the material approaches the limit of plastic deformability, and finally fails at the secondary Lüders-like deformation bands.

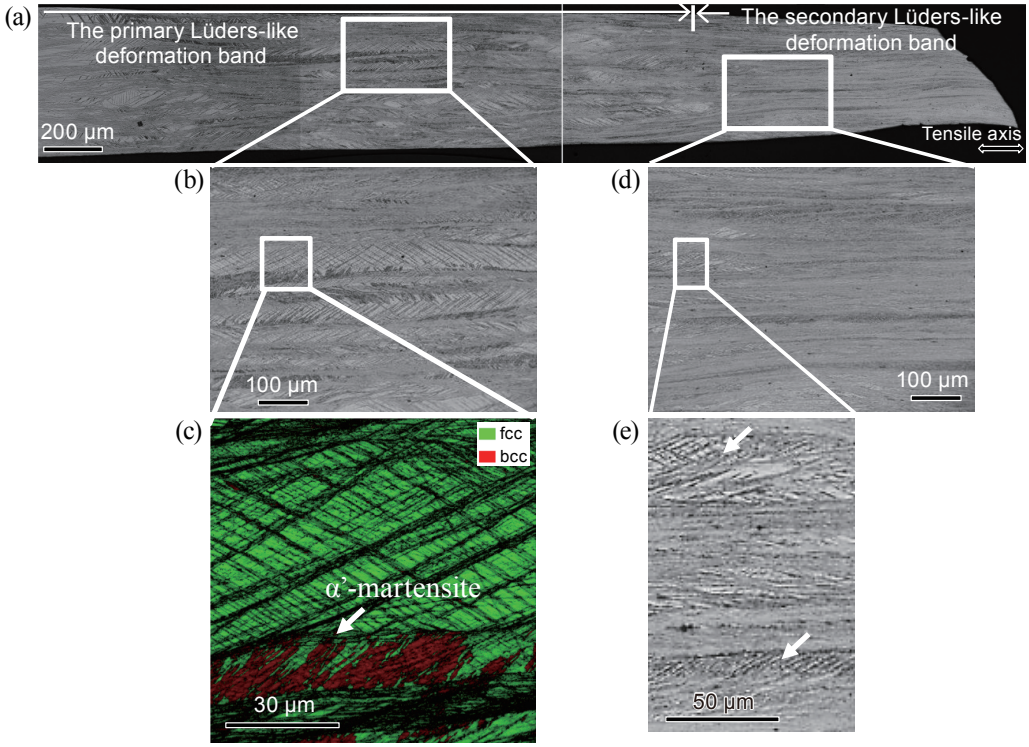

Fig. 10 Microstructure of the 4Al-CR sample after the tensile test:
(a) Aptical micrograph for cross-section of the fractured tensile specimen.
(b) SEM image for the primary Lüders-like deformation bands.
(c) IPF map for the primary Lüders-like deformation bands.
(d) SEM image for the secondary Lüders-like deformation bands.
(e) Highly magnified SEM image for the secondary Lüders-like deformation bands.

4. Discussion

For the Fe-Ni binary system, it has been reported that the value of $(C_{11}\text{-}C_{12})/2$ is lowest at about 30-40% Ni, from experimental data[17-19] and first-principles estimation,[21] which has lowest value of C' depending on alloy composition in the Fe-Ni binary system, corresponds to the phase boundary between the body-centered cubic and fcc phases at ambient temperature. It is also known that lowering the shear modulus, $G_{<011>\ [111]}$, in fcc-based alloys, which can be accomplished by lowering $(C_{11}\text{-}C_{12})/2$, reduces the stacking fault energy (SFE), facilitating the formation of deformation twins.[21] In addition, the starting temperature of martensitic transformation (M_s) in the Fe-Ni binary system drastically decreases with increasing Ni content for Ni content of up to about 40%. The control of M_s, to make the formation of stress-induced martensite start near ambient temperature, was achieved by the addition of proper amounts of aluminum and carbon. Precise alloy design is essential to activate multimodal deformation (dislocation gliding, deformation twinning, and stress-induced martensitic transformation) at ambient temperature.

In addition, the experimental results indicate that the heterogeneous microstructure appears to play an important role in the high ductility (about 40%) at an ultra-high strength level (about 1400 MPa). **Figure 11** shows a schematic illustration of the microstructures formed by severe cold rolling. Multimodal deformation, in the forms of dislocation gliding (Type-A), deformation twins (Type-B), and stress-induced martensitic transformation, operated simultaneously and successively in the material, forming the heterogeneous microstructure. Type-A and Type-B structures seemed to deform preferentially in the subsequent tensile tests via deformation twins and dislocation gliding. The formation of stress-induced martensite near the boundaries between Type-A and Type-C regions was also noted. According to the observation results, the deformation behavior of the heterogeneous microstructure is similar to that of dual-phase steels to some extent. This heterogeneous microstructure leads to high strength and excellent formability, especially in deep drawing. Since the microstructural heterogeneity is contained in the primary Lüders-like deformation bands, as shown in Fig. 10(b), subsequent work hardening and further deformation with secondary Lüders-like deformation bands may occur. The heterogeneity was almost lost in the secondary Lüders-like deformation bands, as shown in Fig. 10(d), samples eventually led to failure.

The heterogeneous microstructure formed by multimodal deformation seems to play an important role in producing the combination of excellent strength and ductility in tensile tests, in which multimodal deformation also occurs. Multimodal deformation can be enabled by precise alloy design to obtain low values of $(C_{11}\text{-}C_{12})/2$, low SFE, and an M_s temperature around ambient temperature.

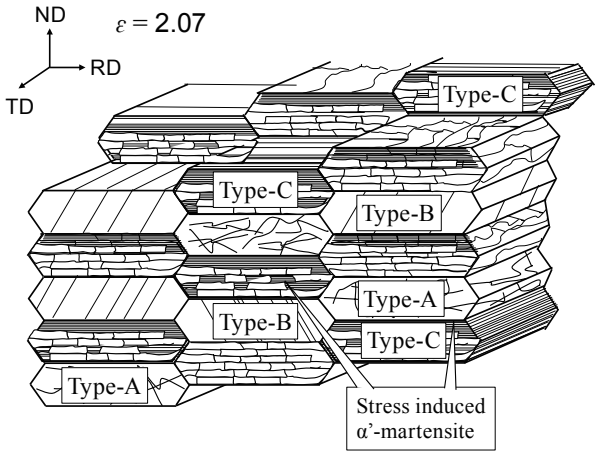

Fig. 11 Schematic illustration of heavily cold rolled microstructure in the 4Al-CR sample.

5. Conclusion

The tensile properties of severely cold-worked Fe-24%Ni-0.45%C-base alloys containing 4% and 6% Al, respectively, and the changes in microstructure during cold rolling and a subsequent tensile test in the Fe-24%Ni-4%Al-0.45%C alloy were investigated. The obtained results can be summarized as follows:

(1) All studied alloys had ultra-high strength and excellent ductility. Among the samples, the Fe-24%Ni-6%Al-0.45%C alloy, which was cold-swaged with an equivalent strain of 2.20 (6Al-SW), showed the highest yield strength (about 2100 MPa). All the alloys showed similar characteristics in their engineering stress-strain curves, i.e., an ultra-high yield strength and yield drop, followed by a plateau with primary Lüders-like deformation, work hardening, and secondary Lüders-like deformation, and finally failure.

The plastic deformation proceeded continuously without plastic instability under such high stress levels.

(2) The sample containing 6% Al consisted of the fcc (γ) matrix and fine particles of the B2 phase (FeNiAl), whereas that containing 4% Al consisted of only the γ phase.

(3) The severely cold-rolled sample containing 4% Al had a quite heterogeneous microstructure. The morphology of the microstructure was classified into the following three types: plain microstructures without any characteristic features, elongated along the rolling direction (Type-A); microstructures containing band-like defects approximately 45° to the normal direction (Type-B); featureless severe plastic deformation structures (Type-C).

(4) As for the microstructural change during cold rolling of the sample containing 4% Al, crystallographic rotation of several degrees inside grains via dislocation gliding was observed for a small strain of $\varepsilon_{CR} = 0.12$. Deformation twins were clearly observed for strains of more than 0.59. The featureless severely deformed region (Type-C) increased for strains (ε_{CR}) of more than 1.06. The formation of the α'-martensite phase was identified in the Type-C structure in the severely cold-rolled sample for strains of up to $\varepsilon_{CR} = 2.07$.

(5) As for the microstructural change during tensile tests of the sample containing 4% Al, fine and dense deformation twins preferentially formed in the Type-A structure, and stress-induced martensitic transformation seemed to occur near the boundaries between Type-A and Type-C structures, or inside the Type-C structure.

(6) Multimodal deformation, in the forms of dislocation gliding, deformation twins, and stress-induced martensitic transformation, operated simultaneously and successively in the material, creating the heterogeneous microstructure. Type-A and Type-B structures seemed to be deformed preferentially in the subsequent tensile tests via deformation twins and dislocation gliding. The formation of stress-induced martensite near the boundaries between Type-A and Type-C, and inside the Type-C structure was also noted.

(7) The heterogeneous microstructure formed by the multimodal deformation seems to play an important role in the excellent combination of strength and ductility observed in the tensile tests, in which multimodal deformation also occurred. The multimodal deformation is enabled by precise alloy design that obtains low values of $(C_{11}-C_{12})/2$, low SFE, and an M_s temperature around ambient temperature.

Reference

(1) Formmeyer, G. et al., *ISIJ Int.*, Vol. 43, No. 3 (2003), pp. 438-446.

(2) Raabe, D. et al., *Adv. Eng. Mater.*, Vol. 11, No. 7 (2009), pp. 547-555.

(3) Guierrez-Urrutia, I. and Raabe, D., *Acta Mater.*, Vol. 59, No. 16 (2011), pp. 6449-6462.

(4) Saito, T. et al., *Science*, Vol. 300, No. 5618 (2003), pp. 464-467.

(5) Furuta, T. et al., *Scr. Mater.*, Vol. 68, No. 10 (2013), pp. 767-772.

(6) Hara, M. et al., *Int. J. Mater. Res.*, Vol. 100, No. 3 (2009), pp. 345-348.

(7) Danno, A. et al., *Mater. Des.*, Vol. 31, Suppl. 1 (2010), pp. S61-S65.

(8) Furuta, T. et al., *Mater. Trans.*, Vol. 46, No. 12 (2005), pp. 3001-3007.

(9) Nagasako, N. et al., *Acta Mater.*, Vol. 105 (2016), pp 347-354.

(10) Kuramoto, S. et al., *Appl. Phys. Lett.*, Vol. 95, No. 21 (2009), 211901-1-211901-3.

(11) Furuta, T. et al., *J. Mater. Sci.*, Vol. 45, No. 17 (2010), pp. 4745-4753.

(12) Furuta, T. et al., *Scr. Mater.*, Vol. 101 (2015), pp. 87-90.

(13) Miyazaki, I. et al., *Mater. Sci. Eng.*, Vol. 721, No. 4 (2018), pp. 74-80.

(14) Ikehata, H. et al., *Phys. Rev. B*, Vol. 70, No. 17 (2004), 174113-1-174113-8.

(15) Morikawa, T. et al., *Mater. Trans.*, Vol. 51, No. 4 (2010), pp. 620-624.

(16) Lu, K. and Hansen, N., *Scr. Mater.*, Vol. 60, No. 12 (2009), pp. 1033-1038.

(17) Charnock, W. and Nutting, J., *Metal Sci. J.*, Vol. 1, No. 1 (1967), pp. 123-127.

(18) Diesburg, D. E., *Doctor Dissertation*, Iowa State University (1971), No. 4446.

(19) Every, A. G. and McCurdy, A. K., *Second and Higher Order Elastic Constants, 1st Edition* (1992), Springer-Verlag Berlin Heidelberg.

(20) Nagasako, N. et al., *Proc. Jpn. Inst. Metals Mater. Spring Meet.* (2009), (CD-ROM).

(21) Izumiyama, M. et al., *J. Jpn. Inst. Metals Mater.*, Vol. 34, No. 3 (1970), pp. 291-295.

(22) Saburi, T. and Wayman, C. M., *Acta Metall.*, Vol. 27, No. 6 (1979), pp. 979-995.

Figs. 2-8
Reprinted and modified from Mater. Des., Vol. 153 (2018), pp. 166-176, Furuta, T., Miyazaki, I., Oh-ishi, K., Kuramoto, S., Shibata, A. and Tsuji, N., Characterization of Cold-rolled Heterogeneous Microstructure Formed by Multimodal Deformation in an Fe-Ni-Al-C Alloy with Lattice Softening, © 2018 Elsevier, with permission from Elsevier.

Figs. 9-10
Reprinted and modified from Mater. Sci. Eng. A, Vol. 721 (2018), pp. 74-80, Miyazaki, I., Furuta, T., Oh-ishi, K., Nakagaki, T., Kuramoto, S., Shibata, A. and Tsuji, N., Overcoming the Strength-ductility Trade-off via the Formation of a Thermally Stable and Plastically Unstable Austenitic Phase in Cold-worked Steel, © 2018 Elsevier, with permission from Elsevier.

Tadahiko Furuta
Research Fields:
- Titanium Based Alloys
- High-strength Metallic Materials
- Powder Metallurgy
- Deformation in Metallic Materials at Near Ideal Strength

Academic Degree: Dr.Eng.
Academic Societies:
- The Japan Institute of Metals and Materials,
- The Iron and Steel Institute of Japan

Awards:
- Technical Development Award, The Japan Institute of Metals and Materials, 1995
- R&D 100 Award, 1996
- Development Award, The Society of Materials Science, Japan, 1999
- Process Development Award, Japan Powder Metallurgy Association, 2000
- Technical Development Award, The Japan Institute of Metals and Materials, 2004

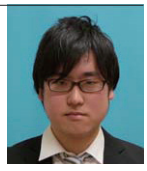

Izuru Miyazaki
Research Fields:
- Strength and Fracture of Materials
- Applied Statistics

Keiichiro Oh-ishi
Research Field:
- Microstructure Characterization

Academic Degree: Dr.Eng.
Academic Societies:
- The Japan Institute of Metals and Materials
- The Japan Institute of Light Metals

Awards:
- Light Metal Advancement Award, The Japan Institute of Light Metals, 2015
- Light Metal Paper Prize, The Japan Institute of Light Metals, 2014

Shigeru Kuramoto*
Research Fields:
- High-strength Metallic Materials
- Deformation in Metallic Materials at Near Ideal Strength

Academic Degree: Dr.Eng.
Academic Societies:
- The Japan Institute of Light Metals
- The Japan Institute of Metals and Materials
- The Iron and Steel Institute of Japan
- The Japan Society of Mechanical Engineers
- The Minerals, Metals & Materials Society

Awards:
- Light Metal Encouragement Prize, The Japan Institute of Light Metals, 2000 and 2014
- Light Metal Paper Prize, The Japan Institute of Light Metals, 2002
- Technical Development Award, The Japan Institute of Metals and Materials, 2004
- Light Metal Advancement Award, The Japan Institute of Light Metals, 2012

Present Affiliation: Ibaraki University

